Available online at www.sciencedirect.com
ScienceDirect
Journal of Solid State Chemistry 180 (2007) 453–460
JOURNAL OF SOLID STATE CHEMISTRY
www.elsevier.com/locate/jssc

Habit modification of calcium carbonate in the presence of malic acid

Zhaofeng Mao, Jianhua Huang*

Department of Chemistry, Zhejiang Sci-Tech University, Hangzhou 310018, PR China

Received 23 August 2006; received in revised form 27 October 2006; accepted 6 November 2006
Available online 9 November 2006

Abstract

The ability of malic acid to control calcium carbonate morphology has been investigated by aging calcium chloride solution in the presence of urea in a 90 °C bath. Malic acid favors the formation of calcite. A transition from single block to aggregate with special morphology occurs upon increasing malic acid concentration. The morphological development of $CaCO_3$ crystal obviously depends on the starting pH. $CaCO_3$ crystal grows from spindle seed to dumbbell in the pH regime from 7 to 11; while it evolves from spindle seed, through peanut, to sphere at pH = 11.5. Both dumbbell and sphere consist of rods that are elongated along *c*-axis and capped with three smooth, well-defined rhombic {1 0 4} faces. A tentative growth mechanism is proposed based on the fractal model suggested by R. Kniep and S. Busch [Angew. Chem. Int. Ed. Engl. 35 (1996) 2624].

Keywords: Calcium carbonate; Calcite; Malic acid; Urea; pH; Morphology

1. Introduction

Biomimetic synthesis and shape-control of $CaCO_3$ crystal has been studied in great detail due to its abundance in nature and also its important industrial application in the paint, plastics, rubber and paper industries [1–5]. Many studies have shown that the properties of calcium carbonate, such as the crystal polymorph, the particle size and shape, are strongly dependent on the preparation methods and additives [6–8]. Organic additives can bind specially to certain crystal planes during crystal growth, thereby modifying the final morphology attained. A wide variety of soluble organic additives were examined for their effects on the crystallization of $CaCO_3$. It was pointed out that the nucleation of $CaCO_3$ was not influenced by the presence of carboxylic acids, but the growth of $CaCO_3$ crystal was reduced by their adsorption to the surface of $CaCO_3$ crystals, which resulted in the variation of crystal polymorph and morphology [9]. It was found that the degree of growth inhibition depended on the number of carboxylic group in the molecule and the amount of the additives added in the system. Propionic acid had no significant influence on the precipitation process, while citric acid completely inhibited the precipitation of vaterite and promoted the formation of calcite [10]. Westin and Rasmuson [11] also pointed out carboxylic acid favored the formation of calcite.

Malic acid with double carboxylic groups also shows a significant influence on the crystal morphology. It influences the crystal morphology even at very low concentrations, producing crystals elongated along [001] direction [12]. A much earlier study showed that small quantities of sodium malate favored the formation of calcite even in the presence of Mg^{2+} ion [13]. Meldrum and Hyde [14] observed a wide range of calcite morphologies produced in the presence of both Mg and organic additives, and a transition from single block to aggregate occurred on increasing the Mg concentration. These morphologies share a feature frequently encountered in biomineralized calcite: orientational ordering, with relative tilt between neighbor crystallites, resulting in curved faces.

On the other hand, the influence of pH on the morphology and structure of crystal has attracted a lot of attention. Cölfen and Qi [15] found the variation of pH drastically changed the morphology of $CaCO_3$ crystal produced in the presence of poly(ethylene glycol)-block-poly(methacrylic acid). Epple's group also reported the

*Corresponding author. Fax: +86 571 88084419.
E-mail address: jhhuang@zstu.edu.cn (J. Huang).

0022-4596/$ - see front matter © 2006 Elsevier Inc. All rights reserved.
doi:10.1016/j.jssc.2006.11.002

morphology of fluoroapatite obtained on titanium and on polymer was clearly dependent on the pH, and two different growth mechanisms at various pHs were proposed [16].

Though the influence of malic acid and pH on the crystal growth is widely studied, the influence of pH on the ability of malic acid to control $CaCO_3$ crystallization is not known. In this work, we studied the effect of malic acid and pH on the crystallization of $CaCO_3$ from $CaCl_2$ aqueous solutions in the presence of urea in a 90 °C bath. It is found that malic acid concentration and the starting pH of solution are important for the final morphology of $CaCO_3$. The development of $CaCO_3$ morphology with the aging time was studied in detail.

2. Experimental section

2.1. Materials and $CaCO_3$ synthesis

All analytical chemicals, calcium chloride, urea, absolute ethanol, sodium hydrate, DL-malic acid (imported from Fisher scientific worldwide company, >99%), were purchased from Hangzhou Huipu Chemical Corporation and used without further purification. All solutions were freshly prepared using doubly distilled water.

$CaCO_3$ particles were precipitated by aging calcium chloride solution in the presence of urea in a 90 °C bath [17]. The reactions were carried out in 50 mL color comparison tubes. Aqueous solutions of $CaCl_2$ (1 M), urea (3 M) and malic acid (1 M) were first prepared as stock solutions. In a typical synthesis, a solution of $CaCl_2$ (1 M, 5 mL) and malic acid (1 M, 1 mL) were added into an aqueous solution of urea (3 M, 10 mL) and diluted to 50 mL under magnetic stirring, Meanwhile, the pH of the solution was adjusted to a desired value (e.g., pH = 9) by using NaOH solution, which gave final $CaCl_2$, urea and malic acid concentrations of 0.1, 0.6 and 0.02 M, respectively. Then the resultant mixture was covered and kept in a 90 °C bath for a certain time (e.g., 4 h). In our experiments, the concentrations of $CaCl_2$ and urea were fixed at 0.1 and 0.6 M, respectively, the starting pH was varied from 7 to 11.5, the concentration of malic acid [MA] was varied from 0 to 40 mM and the aging time was varied from 1 to 12 h. The obtained $CaCO_3$ precipitates were centrifuged and rinsed with doubly distilled water and absolute ethanol, then dried in a vacuum oven at 50° for 24 h and afterwards stored in a desiccator for further characterization.

2.2. Morphological studies and characterization

Scanning electron microscope (SEM) images were taken with JSM-5610 (JEOL, Japan) at 5 or 10 kV, the samples were carefully mounted on copper stubs with double-sided carbon tape and sputter coated with gold before examination. The enlarged SEM pictures were taken with JSM-6700F at 5 kV. The X-ray diffraction patterns were recorded on a X'TRA powder X-ray diffractometer with Cu $K\alpha$ radiation at 40 kV and 120 mA, the scanning step was 0.02° and the 2θ ranged from 10° to 60°. FT-IR measurements were performed on a Nicolet Avatar73 spectrometer on KBr pellets.

3. Results and discussion

3.1. Effect of malic acid concentration

Fig. 1 shows typical SEM pictures of $CaCO_3$ particles precipitated in both the absence and presence of malic acid. Needle-like $CaCO_3$ particles are obtained in the absence of malic acid, as shown in Fig. 1(a). These particles have an average length of about 30 μm with an aspect ratio of ~6. Malic acid shows a strong influence on the crystal morphology and size. When the malic acid concentration [MA] = 0.4 mM, atactic particles with some well-defined faces are gained (Fig. 1(b)). When [MA] is increased to 0.8 mM, particles are elongated along the *c*-axis with length about 50 μm and capped with well-defined {104} faces [18] (Fig. 1(c)). With the further increase of [MA] to 4 mM, particles become further elongated to be about 70 μm, with an aspect ratio ~3 (Fig. 1(d)). Concomitantly, the end {104} faces become smaller, and the linking faces turn to be rounded, which look like spindles. Some small bulges can be observed at the end areas of the spindle. This tendency is basically similar to that reported by Meldrum and Hyde [14]. The anisotropic growth of the particles can be explained by the specific adsorption of organic additives to the particular faces, therefore these additives inhibited the growth of these faces by lowering their surface energy [4]. Surprisingly, the bugles grow into rods if [MA] is further increased to 20 mM, resulting in a dumbbell-like aggregate (Fig. 1(e)). The structure is different from the dumbbell-like Mg-calcite crystals obtained by Meldrum and Hyde [14] in the presence of both Mg and Malic acid. When [MA] is increased to 40 mM, the precipitate looks like two-affixed hemispherical aggregate, as shown in Fig. 1(f).

The crystal polymorphs of products have been investigated through FT-IR and XRD measurements, which are plotted in Figs. 2 and 3, respectively. Curve *a* in Fig. 2 is the FT-IR spectrum of products obtained in the absence of malic acid. The appearance of peak at 1083, 852 cm^{-1} and the pair of bands at 713 and 700 cm^{-1} demonstrates the generation of aragonite [19]. However the broaden small peak near 876 cm^{-1} means a small amount of calcite exists. The results basically agree with the results reported by Matijeević group [17].

The crystal polymorph changes upon the addition of malic acid. Curves *b* and *c* in Fig. 2 show the FT-IR spectrum of resulting precipitates when [MA] is 4 and 20 mM, respectively. The characteristic adsorption bands of aragonite disappear. The bands at 877 and 713 cm^{-1} indicate the particles are calcite, revealing the growth of aragonite is effectively inhibited by malic acid. The presence of malic acid adsorbed on $CaCO_3$ crystals can be examined by FT-IR spectroscopy. Except for the

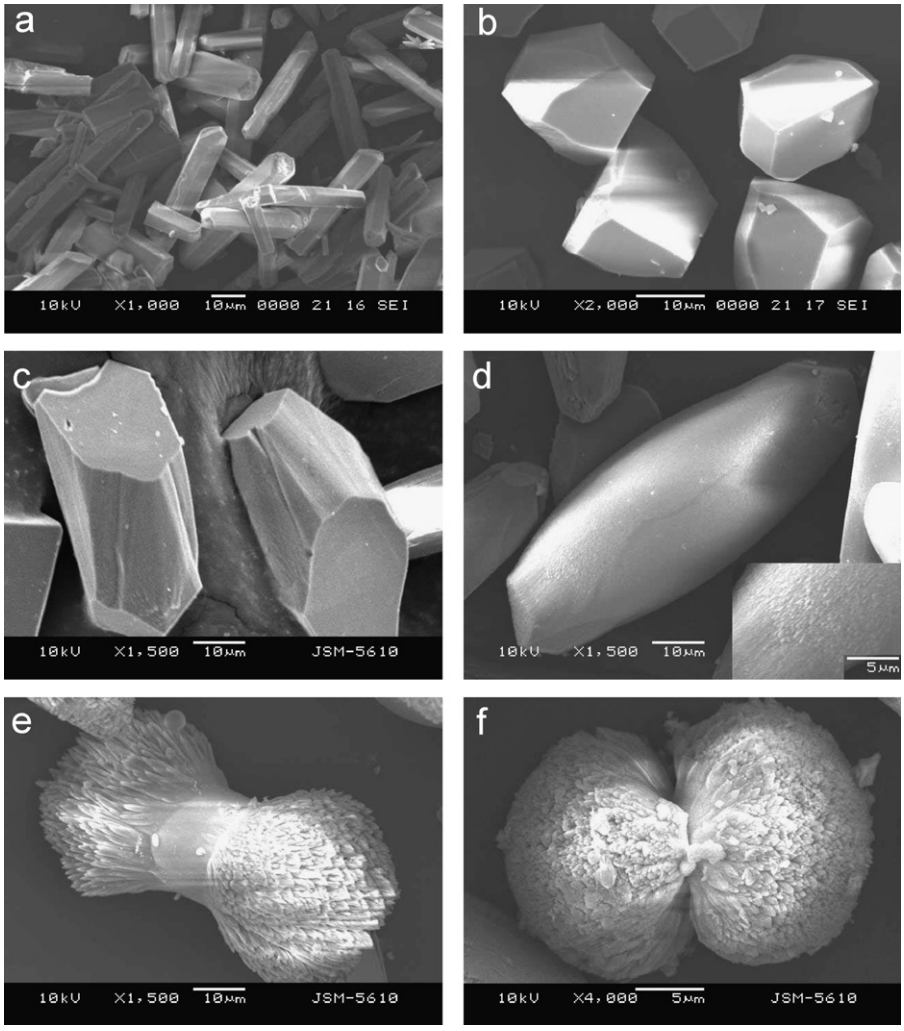

Fig. 1. Typical SEM images of $CaCO_3$ particles obtained in both the absence and presence of malic acid aged for 4 h. pH = 9.0; the malic acid concentration [MA] = (a) 0, (b) 0.4, (c) 0.8, (d) 4, (e) 20 and (f) 40 mM.

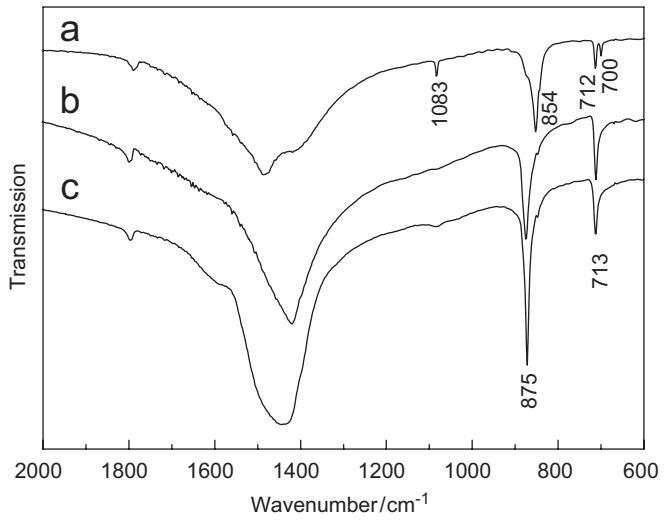

Fig. 2. FT-IR spectra of $CaCO_3$ particles obtained in both the absence and presence of malic acid after being aged for 4 h. pH = 9.0; [MA] = (a) 0, (b) 4 and (c) 20 mM.

absorption bands caused by carbonate ions, the FT-IR spectra of $CaCO_3$ grown in the presence of malic acid seems to show weak adsorption bands around 1600 cm^{-1} characteristic of a carboxylate group [20]. While in their corresponding XRD patterns (Fig. 3), we have not found the diffraction peaks of calcium malate [21]. They exhibit sharp calcite reflections, further proving that the precipitated $CaCO_3$ are calcite crystals. Hence, we deduce that malic acid modifies the growth of $CaCO_3$ by adsorbing onto calcite crystals, instead of producing calcium malate, confirming the speculation made by Wada et al. [9]. Our conclusion is in agreement with an early report that a soluble matrix having carboxylic groups isolated from calcifying cells of alga binds to nuclei rather than to the free Ca^{2+} ions in a solution [22].

3.2. Crystal growth at pH = 7.0 and 11.5

In order to understand the growth mechanism of $CaCO_3$ particles, we have investigated the morphological

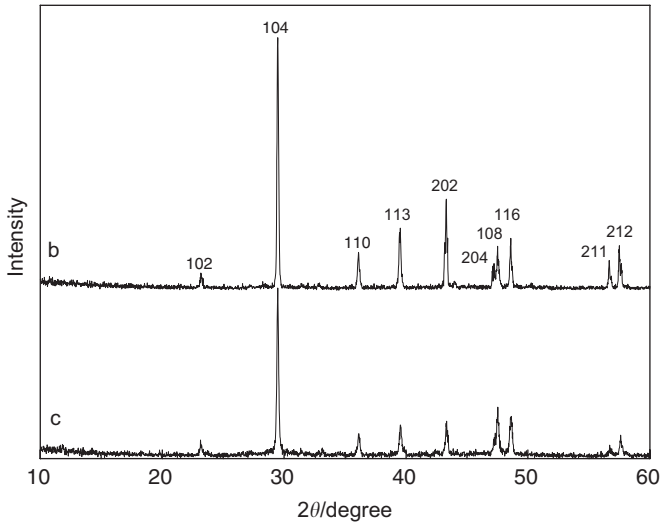

Fig. 3. XRD patterns of $CaCO_3$ particles precipitated after being aged for 4 h. pH = 9.0; [MA] = (b) 4 and (c) 20 mM.

development using SEM analysis by collecting products at various precipitation periods. In this section, since we also want to investigate the effect of pH on the $CaCO_3$ growth, the following experiments are carried out at the same concentration [MA] = 20 mM but at different starting pHs. Here, we present SEM images under two limit conditions: at pH = 7.0 and at pH = 11.5. For the system of pH = 7.0, spherical and spindle-shaped precipitates of about 20 μm in length are observed when the solution is aged for 2.5 h, as shown in Fig. 4(a). As the aging time is prolonged to 4 h, the number of spherical particles decreases, meanwhile the portion and size of spindle-shaped particles with rough ends increase (Fig. 4(b)). The length of spindle is about 30 μm. When the solution is aged for 6 h, lots of needle-like crystals start to grow at the end areas of spindles (Fig. 4(c)). And the average length of the spindles increases to about 50 μm. After it is aged for 12 h, dumbbell-like particles are formed (Fig. 4(d)). It shows that dumbbell-like particles are comprised of a cluster of rods, and the length of the rods changes from shorter than 5 μm to longer than 20 μm.

However, the growth of $CaCO_3$ particle is different at pH = 11.5. At high pH, progressive growth of spindle at both ends leads to peanut and ultimately to spherical aggregate. Also we found that high pH accelerates the growth of crystals: the $CaCO_3$ particles obviously grow faster than those at pH = 7.0. In the earlier period, for instance, aged for 1 h, the peanut-like particles are observed, besides spindle-shaped crystals similar to those obtained after being aged for 4 h at pH = 7.0, however the length of spindle here is only about 5 μm (Fig. 4(e)). When the aging time is prolonged to 2 h, the peanuts grow bigger (Fig. 4(f)). After a longer aging time, such as 6 h, the main morphology is spheres, although a small amount of peanuts still exist (Fig. 4(g). The subunit rods show rough side surface and capped with smooth, well-defined {104} surfaces. While at pH = 7.0, after the same aging time 6 h, such well-capped surfaces are not observed. A prolonged aging time leads to an obvious increase in average particles size. When the aging time increased from 6 to 12 h, spheres become bigger. We measure the particle from a fractured portion and find the rods have grown to about 16 μm in length (Fig. 4(h)). In the whole process, we have not observed the obvious bars on dumbbells which are found at pH = 7.0.

Figs. 5(a) and (b) show enlarged pictures of the needles grown on the spindle after aging for 6 h and rods on the dumbbell after aging for 12 h, respectively, at pH = 7.0. All needles and rods have rough side surfaces. In Fig. 5(b), we can observe the ends of the rods exhibit three smooth, well-defined surfaces indicating the stable calcite {104} surfaces [14]. However, such smooth capped surfaces have not been found in Fig. 5(a). Capped {104} surfaces on some rods are observed when the aging time reached 8.5 h. Therefore, we speculate that the regular rhombic rods are not formed at the early stage but developed from the needles. We also find the morphology of crystal will not continue to change as soon as the smooth {104} surfaces are formed.

3.3. *Influence of starting pH*

The above SEM results clearly show that the starting pH of solution has an obvious influence on the morphologies of the precipitated $CaCO_3$ crystals. Combined with the results at other pHs, such as shown in Fig. 6, it is discovered that dumbbell-like particles possessing a smooth bar at their central region are produced in the pH regime from 7.0 to 11.0. With an increase of the starting pH, the bar length decreases and ultimately disappears with further increase of pH to be 11.5, eventually resulting in the formation of spheres. Cölfen and Qi [23] also reported that the variation of pH drastically changed the morphology of the produced $CaCO_3$ crystal in the presence of double hydrophilic block copolymer. They also presented a morphology map for the rod-dumbbell-sphere transition of calcite as pH was changed from 9 to 11.

We find pH also influence the polymorph of $CaCO_3$. Fig. 7 gives XRD patterns of products precipitated at pH = 7.0 and 11.5 after being aged for 12 h, respectively. Curve *a* shows $CaCO_3$ obtained at pH = 7.0 contains a little vaterite. While at pH = 11.5, the products are pure calcite (curve *b*).

The above observations demonstrate that the morphology of $CaCO_3$ obviously depends on the reaction time, the starting pH, and [MA]. As shown in Fig. 8, dotted arrows I and II represent the morphological changes due to the prolongation of reaction time at the starting pH value of 7.0 and 11.5, respectively. Dotted arrows III and IV reveal the morphological development of calcite with the increase of the starting pH value and [MA], respectively.

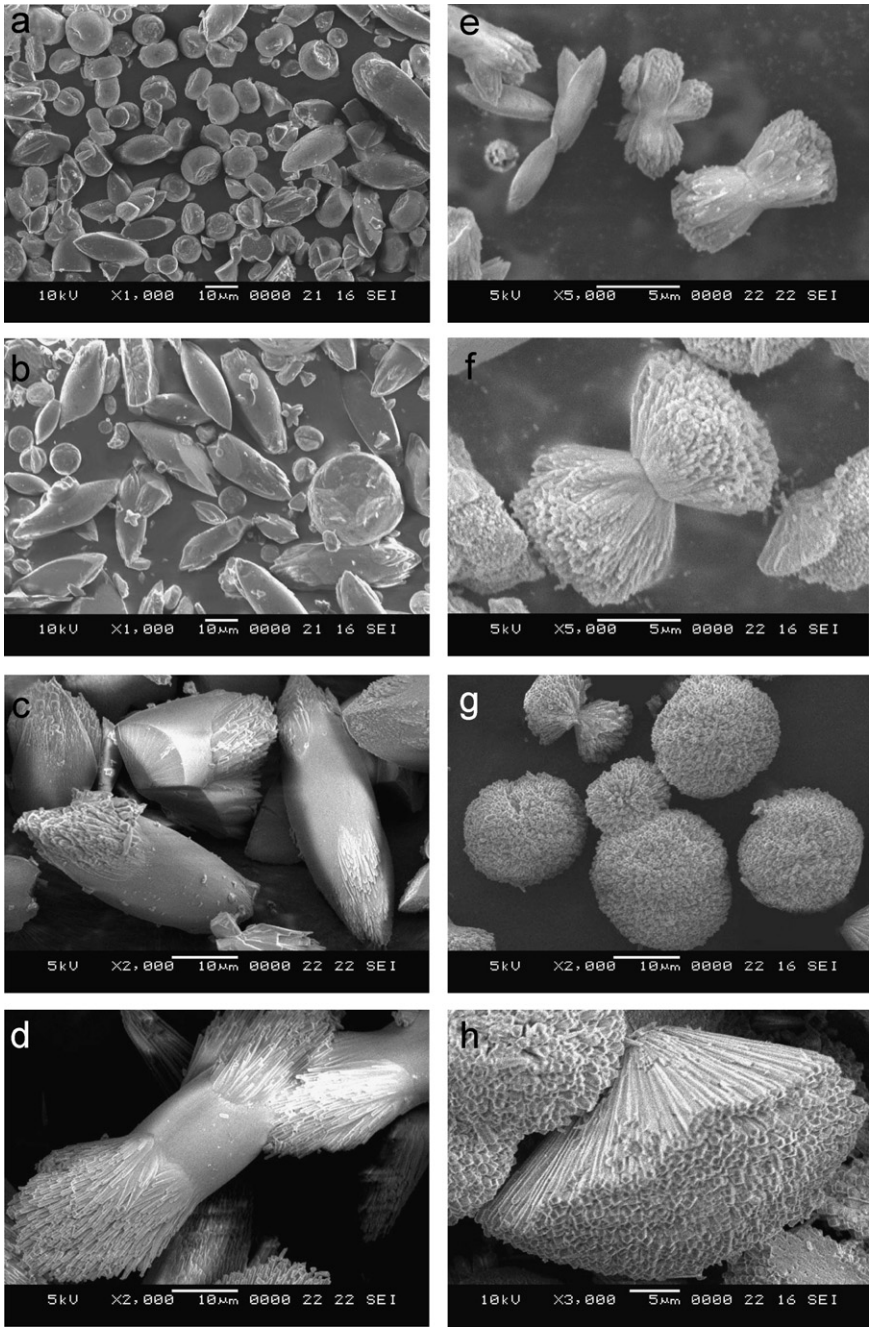

Fig. 4. SEM images of $CaCO_3$ particles precipitated at various periods, [MA] = 20 mM. Left: pH = 7.0, the solution was aged for (a) 2.5 h, (b) 4 h, (c) 6 h, and (d) 12 h. Right: pH = 11.5, the solution was aged for (e) 1 h, (f) 2 h, (g) 6 h and (h) 12 h.

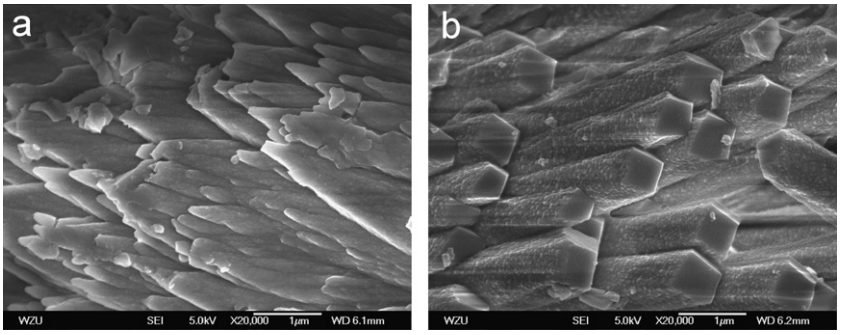

Fig. 5. Enlarged SEM images of products obtained at pH = 7.0. [MA] = 20 mM. The solution was aged for (a) 6 h and (b) 12 h.

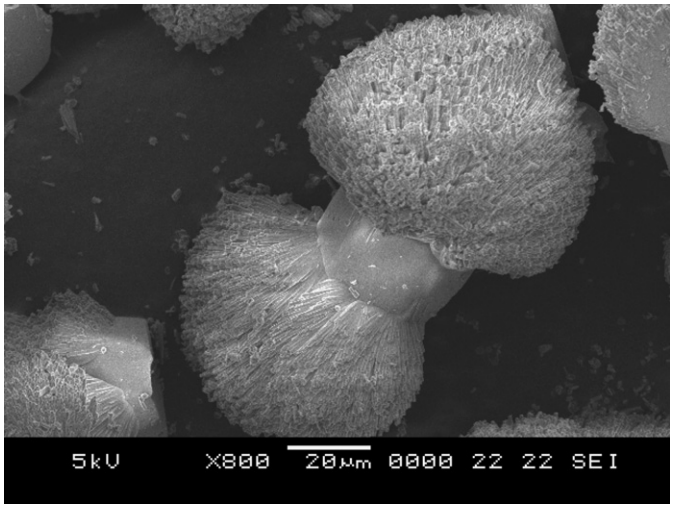

Fig. 6. SEM image of $CaCO_3$ particles obtained after being aged for 12 h. [MA] = 20 mM; pH = 11.0.

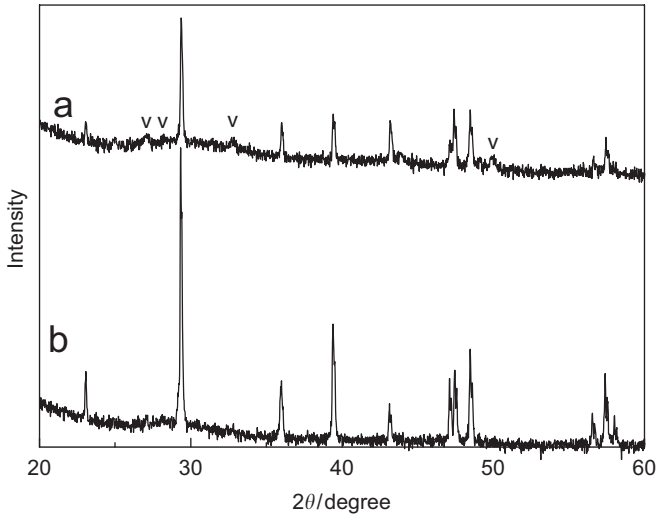

Fig. 7. XRD patterns of $CaCO_3$ particles obtained after being aged for 12 h. [MA] = 20 mM; pH = (a) 7.0 and (b) 11.5. "V" denotes peaks from vaterite.

3.4. Growth mechanism

The above sequence of morphology growth from spindles, through peanuts, to spheres seems to be a general growth phenomenon and has been observed for several systems [16,24–26]. Chen et al. [26] prepared $CaMoO_4$ and $SrMoO_4$ by the reaction of metal and molybdate ions in alkaescent aqueous solution in the absence of any surfactant or template. A distinct morphology transformation from ellipsoidal rods, to peanuts, dumbbells, peaches and grown spherules was observed. They indicated that pH value of the solution did not have a crucial influence on the shape evolution of products. However, Epple's group [16] has shown that the morphology obviously depended on pH after carrying out the crystallization of fluoroapatite on titanium or on polymer in the absence of organic additive. A similar morphology evolution was found; nevertheless their experiments were performed at lower pH.

Kniep and Busch [25] reported the growth of the fluorapatite spheres by double diffusion in gelatin that begins from an elongated hexagonal-prismatic seed. Progressive stages of self-assembled (noncrystallographic) upgrowth of needle-like prisms at both ends of the seed (fractal branching) lead to dumbbell-like aggregates that complete their shapes by successive and self-similar upgrowth to give notched spheres. They proposed a fractal growth model where the architecture is controlled by two noncrystallographic parameters: (i) the divergent angle between the prism axis of the growing crystals and the prism axis of the preceding seed crystal; (ii) the number of subsequent generations.

Based on the fractal growth model [25,27], a tentative growth mechanism is figured in Fig. 9. We divide the whole growth process into three stages. The spindle seeds form in the first stage. In stage II, some bulges begin to appear at the ends of spindle seeds. These bulges finally grow into needles whose side-faces also provide some new growth sites for subunit needles, as shown in Fig. 5(a). Each needle of all generations is capped with three smooth, well-defined {104} surfaces in stage III. Our results indicate that the morphology of the crystal will not continue to change once the smooth {104} surfaces are formed. Similar but bigger particles could be obtained by further prolonging the aging time (Fig. 4(h)). Obviously, stage II controls the morphology of particles. We speculate that the crystal morphologies may be affected by three parameters: (i) the growth sites of bulges, (ii) the divergent angle between the long axis of spindle and the grown bugle-axis (just as α or β shown in Fig. 9), (iii) the number of generations. In the present work, the term 'generations' is adopted from the fractal model proposed by Kniep and Busch [25,27]. Growth of bulge from the spindle is called the first generation. The subsequent growth of subunit needle from bulge is called the second generation. And the further self-similar growth of the second-generation needle is called the third generation. The rest may be deduced by analogy. Compared with the condition of low pH, the growth sites of bulges under the high pH condition spread to the middle of spindle seeds, leading to the formation of dumbbells without bars (Fig. 4(f)), Meanwhile the larger angle ($\beta > \alpha$) and much more generations accelerate the growth of spherical particles. The angle α and β may be relevant to the selective adsorption of malic acid to calcite surface steps, as indicated in Ref. [28].

4. Conclusion

In summary, the effect of malic acid on the precipitation of $CaCO_3$ by aging calcium chloride solution in the presence of urea in a 90 °C bath has been studied in detail. Malic acid favors the formation of calcite. The malic acid

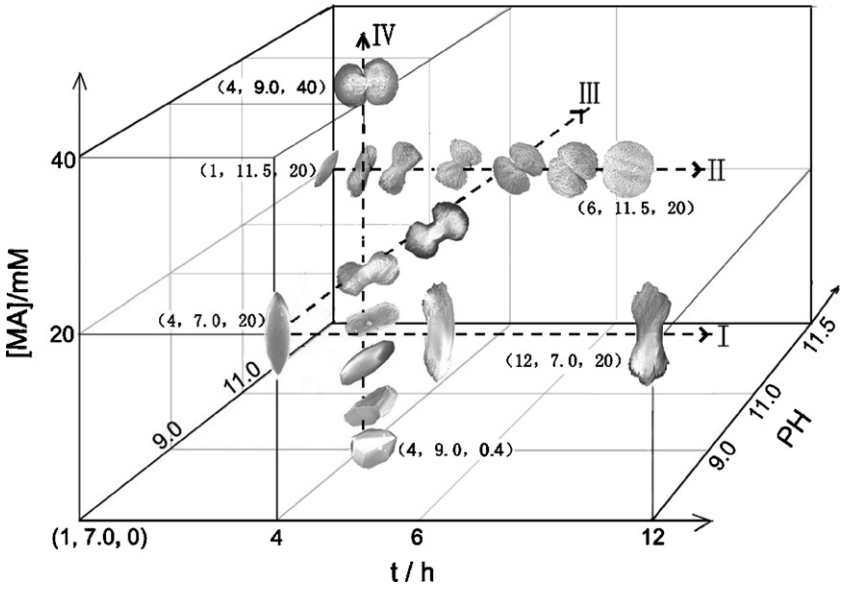

Fig. 8. Dependence of the morphology of $CaCO_3$ on the reaction time t, pH and concentration of malic acid [MA]. The particles' size shown in the map is not to scale.

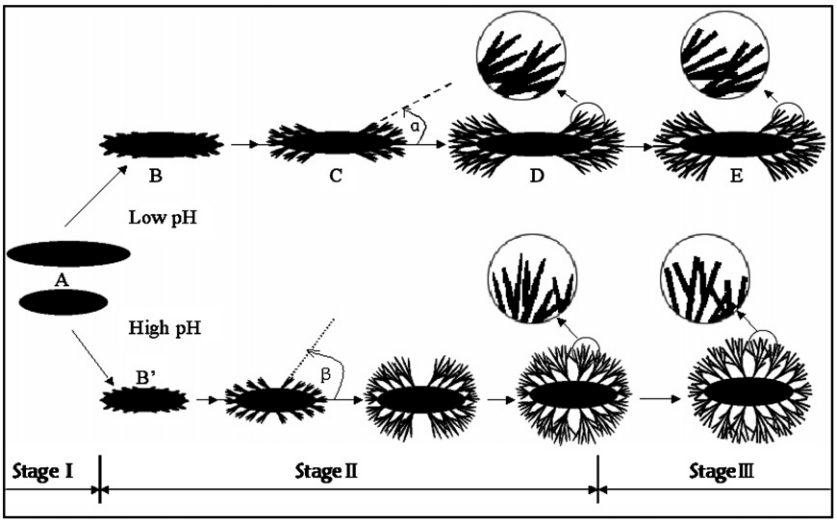

Fig. 9. A tentative model for the dumbbell-like growth at pH = 7.0–11.0 (as shown in Fig. 4, left) and sphere-shaped growth at pH = 11.5 (as shown in Fig. 4, right).

concentration and the starting pH of the solution are two important parameters controlling the final morphologies of $CaCO_3$. A transition from single block to aggregate with special morphology occurs upon increasing the concentration of malic acid. The morphological development of $CaCO_3$ crystal obviously depended on the starting pH. At pH between 7.0 and 11.0, $CaCO_3$ crystal grows from spindle-shaped seed to dumbbell-like aggregate; while when pH reaches 11.5, it evolves from spindle-shaped seed, through peanut, and ultimately to sphere. Both dumbbell and sphere consist of rods that are elongated along c axis and capped with three smooth, well-defined calcite {104} faces. A tentative growth mechanism is proposed based on the fractal model suggested by Kniep and Busch [25].

Acknowledgment

The work was supported by the Natural Science Foundation of China under Grant no. 20571065.

References

[1] S. Mann, G.A. Ozin, Nature 382 (1996) 313.
[2] S.F. Chen, S.H. Yu, T.X. Wang, J. Jiang, H. Cölfen, B. Hu, B. Yu, Adv. Mater. 17 (2005) 1461.
[3] H. Cölfen, Curr. Opion. Colloid Interface Sci. 8 (2003) 23.
[4] S.H. Yu, H. Cölfen, J. Mater. Chem. 14 (2004) 2124.
[5] H. Cölfen, M. Antonietti, Angew. Chem. Int. Ed. 44 (2005) 5576.
[6] K. Naka, Y. Chujo, Chem. Mater. 13 (2001) 3245.
[7] T. Kato, A. Sugawara, N. Hosoda, Adv. Mater. 14 (2002) 869.
[8] J.G. Yu, M. Lei, B. Cheng, X.J. Zhao, J. Solid State Chem. 177 (2004) 681.

[9] N. Wada, K. Kanamura, T. Umegaki, J. Coll. Interface Sci. 233 (2001) 65.
[10] N. Vdović, D. Kralj, Coll. Surf. A: Physicochem. Eng. Aspects 161 (2000) 499.
[11] K.J. Westin, A.C. Rasmuson, J. Coll. Interface Sci. 282 (2005) 359.
[12] T.K. Anee, N.M. Sundaran, D. Arivuoli, P. Ramasamy, S.N. Kalkura, J. Crystal Growth 285 (2005) 380.
[13] Y. Kitano, D.W. Hood, Geochim. Cosmochim. Acta. 29 (1965) 29.
[14] F.C. Meldrum, S.T. Hyde, J. Crystal Growth 231 (2001) 544.
[15] H. Cölfen, L.M. Qi, Chem. Eur. J. 7 (2001) 106.
[16] O. Prymak, V. Sokolova, T. Peitsch, M. Epple, Crystal Growth Des. 6 (2006) 498.
[17] L.f. Wang, I. Sondi, E. Matijević, J. Colloid Interface Sci. 218 (1999) 545.
[18] J. Aizenberg, S. Albeck, S. Weiner, L. Addadi, J. Crystal Growth 142 (1994) 156.
[19] G.T. Zhou, J.C. Yu, X.C. Wang, L.Z. Zhang, New Chem. J. 28 (2004) 1027.
[20] N. Wada, K. Yamashita, T. Umegaki, J. Colloid Interface Sci. 212 (1999) 357.
[21] T. Jini, K.V. Sahan, G. Varghese, Cryst. Res. Technol. 40 (2005) 1155.
[22] Ah. Borman, E.W. de Jong, M. Huizing, D.J. Kok, P. Westbroek, L. Bosch, Eur. J. Biochem. 129 (1982) 179.
[23] H. Cölfen, L.M. Qi, Chem. Mater. 12 (2000) 2392.
[24] S.H. Yu, H. Cölfen, M. Antonietti, J. Phys. Chem. B. 107 (2003) 7396.
[25] R. Kniep, S. Busch, Angew. Chem. Int. Ed. Engl. 35 (1996) 2624.
[26] D. Chen, K.B. Tang, F.Q. Li, H.G. Zheng, Crystal Growth Des. 6 (2006) 247.
[27] S. Busch, H. Dollhaine, A. DuChesne, S. Heinz, O. Hochrein, F. Laeri, L. Pdebrad, U. Vietze, T. Weiland, R. Kniep, Eur. J. Inorg. Chem. 10 (1999) 1643.
[28] C.A. Orme, A. Noy, A. Wierzbicki, M.T. McBride, M. Grantham, H.H. Teng, P.M. Dove, J.J. DeYoreo, Nature 441 (2001) 775.